Analyst

ROYAL SOCIETY OF CHEMISTRY

PAPER

View Article Online
View Journal | View Issue

Cite this: *Analyst*, 2025, **150**, 1578

A point-of-need framework for illicit drug identification with high-resolution mass spectrometry†

Thomas P. Forbes, *[a] Elizabeth L. Robinson, [a] Edward Sisco [a] and Abigail Koss[b]

The continually evolving drug landscape, with novel synthetic drugs and unique compositions, necessitates the need to advance technologies, data analysis methods, and data accessibility for compound detection and identification. Providing public health, first responder, and law enforcement communities with critical information in near real-time will aid emergency response and public awareness, and direct overdose prevention and interdiction efforts. A major component of this framework is the progression of accurate drug screening and preliminary identifications from a more rigid laboratory-based arrangement to an agile point-of-need paradigm. We investigated drug detection and identification of a field deployable ruggedized high-resolution time-of-flight mass spectrometer, employing both acetone-assisted vacuum ultraviolet (VUV) photoionization and dielectric barrier discharge ionization (DBDI) schemes. This preliminary fit-for-purpose exploration was conducted under laboratory conditions, considering ion sources not reliant on helium gas or external roughing pumps, building toward deployment in a mobile laboratory setting. The chromatography-free measurements enabled rapid analysis of neat drug solutions and multi-component mixtures. Characterization and optimization of system parameters demonstrated sensitive performance, with limits of detection in the tens to hundreds of picograms for a range of drug classes from multiple-component mixtures. The system's high mass resolution was calibrated with a polyethylene glycol calibrant, enabling accurate matching with spectral library entries. Integrating compound identification with the NIST DART-MS Forensics Database and NIST/NIJ DART-MS Data Interpretation Tool provided a solid foundation for transition to the point-of-need. The overarching framework seeks to support technology advancement and adoption, as well as the development of novel data analysis tools, processes, and management for public access and utilization.

Received 23rd January 2025,
Accepted 15th March 2025

DOI: 10.1039/d5an00082c

rsc.li/analyst

Introduction

The development of measurement science and standards aimed at supporting the public health, first responder, law enforcement, and forensic science communities remains critical to combating the drug overdose epidemic.[1] At the foundation of this support is the chemical analysis of samples, leading to accurate identification or classification of illicit drug composition. Advancements in analytical technology, novel data analysis algorithms, and growing chemical libraries and datasets are bolstering a move from laboratory-based analysis to on-site measurement.[2,3] This shift enables near real-time feedback – in the form of chemical identification(s) – to first responders or harm reduction personnel, containing crucial information for individual and community safety.

On-site detection and identification of illicit drugs is dominated by the use of color tests[4] and lateral flow immunoassay (test strips),[5] both supported by advancement in paper-based microfluidics;[6] as well as spectroscopy-based techniques like Raman and Fourier transform infrared (FTIR) due to their low cost, ease of use, and portability.[7] These techniques, however, are non-ideal for obtaining high-quality data on drug samples that are often complex mixtures. Color tests have been shown to frequently produce inconclusive or incorrect results, and color changes of novel psychoactive substances and new synthetic opioids are not well documented.[8] Test strips provide information about a specific drug or class of drugs – presenting a narrow piece of information – and are prone to cross-reactivity.[9] Spectroscopy techniques often cannot reliably

[a]*National Institute of Standards and Technology, Materials Measurement Science Division, Gaithersburg, Maryland 20899, USA. E-mail: thomas.forbes@nist.gov*
[b]*TOFWERK USA, Boulder, Colorado 80301, USA*

†Electronic supplementary information (ESI) available: Additional experimental method details, ionization pathways, response curves, mass spectra, and figures as noted in the text. See DOI: https://doi.org/10.1039/d5an00082c

detect minor components in a mixture. These minor components are critical to detect in drug mixtures as they often present the highest danger.

While the limited data that color tests, test strips, and spectroscopy-based techniques provide are useful, they do not allow law enforcement, harm reduction personnel, or people who use drugs with a way to fully understand the dangers present within a sample. Because of this, many agencies rely on sending samples to laboratories for additional, comprehensive analysis using a mass spectrometry-based approach. While this approach provides useful data for monitoring the illicit drug landscape, the time delays caused by shipping the sample and backlogs at laboratories render the information obsolete for the person who initially provided the sample. Over the past few years, efforts to close the time-gap on comprehensive drug product testing have been undertaken using rapid laboratory-based analyses,[10] on-site analyses using laboratory-grade mass spectrometers,[11] and mobile analyses[12] using laboratory-grade mass spectrometers.

The sensitive and selective detection capabilities of mass spectrometry (MS) have made it a premier analytical technique for chemical identification from complex mixtures. Instrumentation advancements and miniaturization have yielded a range of fieldable mass spectrometers[13–15] – from high-pressure ion traps[16] to time-of-flight (TOF) analyzers.[17,18] The evolution of portable mass spectrometers has coincided with the vast expansion in ambient and atmospheric pressure ionization techniques.[19–21] The versatility of these ionization sources and simplicity of coupling with a variety of sample introduction avenues has enabled a plethora of adaptable fit-for-purpose front-end configurations[22–24] that have been applied to innumerable applications.[22,23,25–27]

In response to the needs of the public health and forensic communities, and areas highlighted by the U.S. TRANQ Research Act[28] and U.S. Office of National Drug Control Policy,[29] we investigated the identification of illicit drugs with a rugged high-resolution TOF mass spectrometer. This investigation is an extension of the National Institute of Standards and Technology (NIST) rapid drug analysis and research (RaDAR) program.[30,31] The RaDAR program works with local, state, and federal partners to monitor the chemical composition of the drug landscape. Here, characterization of sample introduction, ionization pathways, and MS performance was conducted for a 15-component drug mixture and nine (9) single-component drug solutions. The chromatography-free analysis employed the thermal desorption of extracted samples coupled with either dielectric barrier discharge ionization (DBDI) or acetone-assisted vacuum ultraviolet (VUV) photoionization, sources free from potential needs for helium gas or external pumping. Ionized samples were analyzed by a relatively compact transportable TOF mass spectrometer that has been designed, deployed, and demonstrated sensitive measurements for on-site, mobile, and field applications.[18,32,33] Parametric and performance characterization was followed with an analysis of compound identification, exploiting related data tools – specifically, adapting analysis to the NIST DART-MS Forensics Database (an illicit drug centric MS library comprised of spectra collected with direct analysis in real time [DART] ionization) and NIST/NIJ DART-MS data interpretation tool (spectral matching algorithm). These studies lay the foundation toward rapid near real-time drug screening and preliminary identification at the point-of-need to aid in monitoring the drug landscape.

Methods

Materials

A standard mixture solution containing an array of fifteen drugs – each at 250 μg mL^{-1} in methanol – was purchased from Cayman Chemical (GC-MS Drug Standard Mixture 4, Ann Arbor, MI, USA)‡. The mixture was comprised of cathinones: α-pyrrolidinobutiophenone (α-PBP), α-pyrrolidinopentiophenone (α-PVP), ethylone (3,4-methylenedioxy-*N*-ethylcathinone or βk-MDEA), and butylone (β-keto-*N*-methylbenzodioxolylbutanamine or βk-MBDB); arylcyclohexylamines: tenocyclidine (TCP) and phencyclidine (PCP); stimulants: cocaine and methamphetamine; an opiate: heroin; synthetic opioids: furanyl fentanyl and furanyl fentanyl 3-furancarboxamide isomer; benzodiazepine: alprazolam; steroids: nandrolone and stanozolol; and a synthetic cannabinoid: 5-fluoro ADB (5-fluoro MDMB-PINACA). Single-component standards for methamphetamine, α-PBP, tenocyclidine, furanyl fentanyl, heroin, alprazolam, *N*,*N*-dimethylpentylone (*N*,*N*-DMP), fentanyl, and cocaine were also purchased from Cayman Chemical. Standard solutions were gravimetrically or volumetrically diluted in liquid chromatography (LC)-MS Chromasolv grade acetonitrile (Sigma-Aldrich, St. Louis, MO, USA) for further use. A selection of three (3) samples from the NIST RaDAR program were also analyzed for real-world demonstration. These samples were collected from used drug paraphernalia at harm reduction sites on the U.S. east coast and returned to NIST for extraction and analysis.[10] Details of sample collection and preparation can be found in the literature.[10] Briefly, *meta*-aramid wipes or cotton swabs were used to swipe the external surfaces of paraphernalia. Collection media (*i.e.*, wipes and or swabs) were placed into coin envelopes and returned to NIST, where they were extracted in 1 mL acetonitrile and vortexed. Melting point capillary tubes were used as sampling substrates for dissolved drug solutions or solvent-extracted collections.

Instrumentation

Analyte-laden sample substrates (*e.g.*, melting point capillaries) were inserted into a GC interface heater (GC/SPME Module, Plasmion GmbH, Augsburg, Germany) operated at 250 °C unless noted (temperatures from 180 °C to 300 °C were

‡Certain commercial equipment, instruments, or materials are identified in this article in order to specify the experimental procedure adequately. Such identification is not intended to imply recommendation or endorsement by NIST, nor is it intended to imply that the materials or equipment identified are necessarily the best available for the purpose.

investigated). Following thermal desorption, vaporized analytes were ionized by either an in-line dielectric barrier discharge ionization (DBDI) source (SICRIT [soft ionization by chemical reaction in transfer], Plasmion GmbH, Augsburg, Germany)[34] or high-pressure acetone-adduct chemical ionization source (Aim reactor, TOFWERK AG, Thun, Switzerland).[35] All hardware configurations were mounted on a Vocus S time-of-flight (TOF) mass spectrometer (TOFWERK). This class of instruments has been frequently deployed for mobile applications and come in a range of sizes, mass resolving power, and system requirements.[18,32,33] The mass spectrometer was approximately 64 cm deep × 50 cm wide (62 cm with wheels) × 114 cm high, weighing approximately 120 kg and requiring standard 120 V (60 Hz) and 1 kW power. Custom mounting brackets are available for future deployment in a vehicle. The TOF mass spectrometer front-end hardware contained a sampling inlet separated by a pressure-reducing orifice from an ion-molecule reactor chamber. The ion-molecule reactor was followed by a series of RF-only quadrupole ion guides and focusing elements to accomplish differential pumping and interface with the mass analyzer. In the "Aim reactor" configuration, acetone chemical ionization reagent ions were introduced directly into the ion molecule reactor using a krypton vacuum ultraviolet (VUV) lamp (operated at 1600 V unless noted, with voltages from 900 V to 2000 V investigated) and reagent gas from a heated acetone permeation tube. In DBDI configuration, the DBDI source was mounted on the inlet, in front of the ion molecule reactor. The "Aim reactor" hardware (*i.e.*, krypton lamp and permeation tube heater) remained in place for DBDI operation but were powered OFF. Details of the in-line DBDI source can be found in the literature.[34,36–38] Briefly, a concentric electrode geometry generated a stable plasma for ionization between a thermal desorption unit and the MS inlet. Unless noted, the DBDI source was operated at 1400 V and 15 kHz, with the voltage range 1100 V to 1600 V investigated. Following thermal desorption and ionization, ions were focused and guided into an orthogonal reflectron TOF, impacting a multichannel plate detector.

Safety considerations

Safety data sheet recommendations and standard practices were followed for storage and handling of hazardous materials (*e.g.*, drug compounds). In this work, hazardous samples were already dissolved in solution. A portable fume extractor (containing carbon and HEPA filters) was used around the thermal desorber, and mass spectrometer pumps were appropriately vented through the building ventilation.

Results and discussion

We explored the coupling of multiple sample introduction and ionization methods with a rugged TOF mass spectrometer to define critical parameters for on-site drug detection and identification. This investigation builds upon existing work of the NIST RaDAR program[30,31] (Fig. 1), for which samples collected by local, state, or federal partners are shipped back to NIST for analysis. Here, we explore instrumentation for moving toward point-of-need drug identification, drug landscape monitoring, and associated public health applications (Fig. 1). For example, sample chemical composition could be provided at harm reduction sites or other points-of-need in near real-time, mapping the drug landscape. Bringing the laboratory to the point-of-need will remove the need for sample packaging and shipping (Step 2), a main contributor to the lengthy turn-around time. Similarly, ongoing and future avenues are considering removal of the solvent extraction step (Step 3) and directly analyzing wipes or paraphernalia-dipped glass capillaries. Here, we used a cause-and-effect analysis to aid in identifying critical process parameters (CPPs) impacting both measurement variability and compound identification confidence. An Ishikawa diagram laid out the major processes

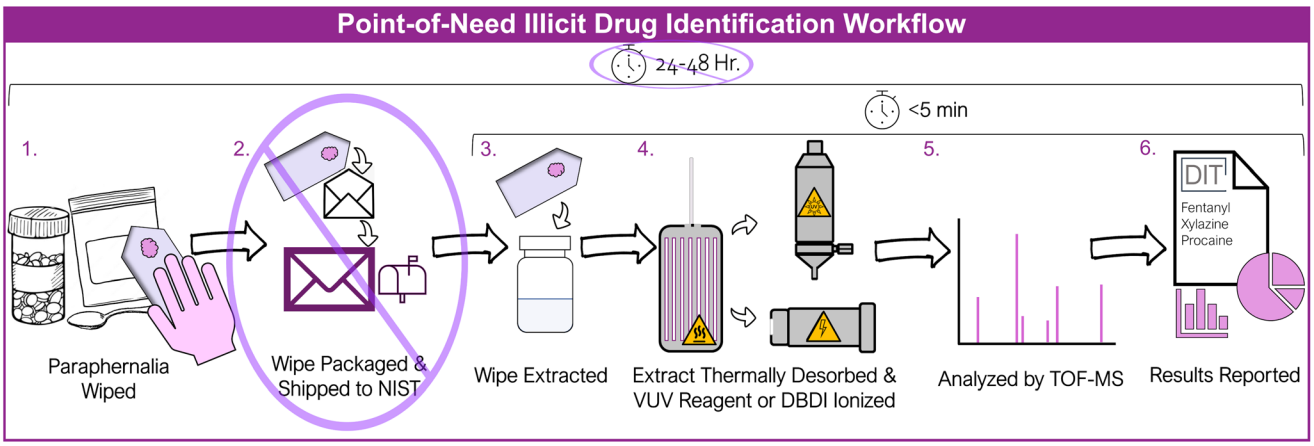

Fig. 1 Schematic representation of the NIST RaDAR workflow and overall reduction in process time by on-site analysis. Step 1: swipe sample collection from paraphernalia, 2: packaging of sample-laden wipes and shipping to NIST, 3: solvent extraction of wipes, 4: thermal desorption and ionization of samples, 5. TOF-MS analysis, and 6. Library matching and preliminary identification.

in compound identification – from sample collection to library matching – and established the main factors (and their relationships) impacting compound detection and identification (Fig. S1†). Critical process parameters for detailed investigation were chosen from this analysis and prior experience.

Mass spectrometry detection CPPs

The process parameters investigated here were related to sample introduction, entrainment, ionization, transmission, and detection. The initial processes in mass spectrometric compound detection and identification revolve around sample introduction to the gas phase and analyte ionization (Fig. S1† – first two branches of the cause-and-effect diagram).

Sample introduction. The presented workflow considered traditional swipe or swab sample collection of paraphernalia, followed by a solvent extraction.[10] Many factors impact sample collection and extraction efficiencies, from force applied and wipe material to extraction solvent and method, and have been studied in detail.[39–41] Likewise, the thermal desorption of organic compounds such as drugs, excipients, and explosives generally follow trends corresponding to compound volatility (*e.g.*, vapor pressure).[42–44] The transportable TOF instrument employed here demonstrated similar relationships between MS response and increasing thermal desorption temperatures (Fig. S2†) – more volatile compounds such as methamphetamine yielded optimal vaporization at lower temperatures than less volatile compounds such as furanyl fentanyl. Sample thermal desorption was predominantly affected by the compound physicochemical properties (*e.g.*, spatial distribution or vapor pressure), with relatively consistent trends across sample introduction or thermal desorber configurations.

Sample entrainment and transport. Mass spectrometry front-end configurations often utilize the instrument vacuum for transport to, and through, the inlet. However, various forms of aerodynamically assisted transport using vacuum pumps, the venturi effect, and related aerosol or vapor sampling systems have become more prominent.[45,46] These platforms aid sample collection and transport, as well as playing a role in ion-sample proximity and interaction time (Fig. S1†). The Vocus S instrument employed here included an interface with concentrically pulling flow, driven by an internal membrane pump, to aid in sample entrainment (Fig. S3†). In combination with the backing and turbomolecular pumps maintaining vacuum within the instrument, the inlet pump supported the flow of sample through the thermal desorber and in some cases the DBDI source (Fig. 2(a) and (b)) and into the reactor region, upstream of the quadrupole ion guides. Optimal pull from the inlet pump (based on maximum analyte signal) depended on the aerodynamic resistance of the upstream configuration. For example, a configuration with the capillary sample thermal desorber mounted directly onto the inlet required no additional flow support for analyte entrainment (Fig. 2(c-i)). Excess aerodynamic flow from the inlet pump demonstrated reduced signal, attributed to losses

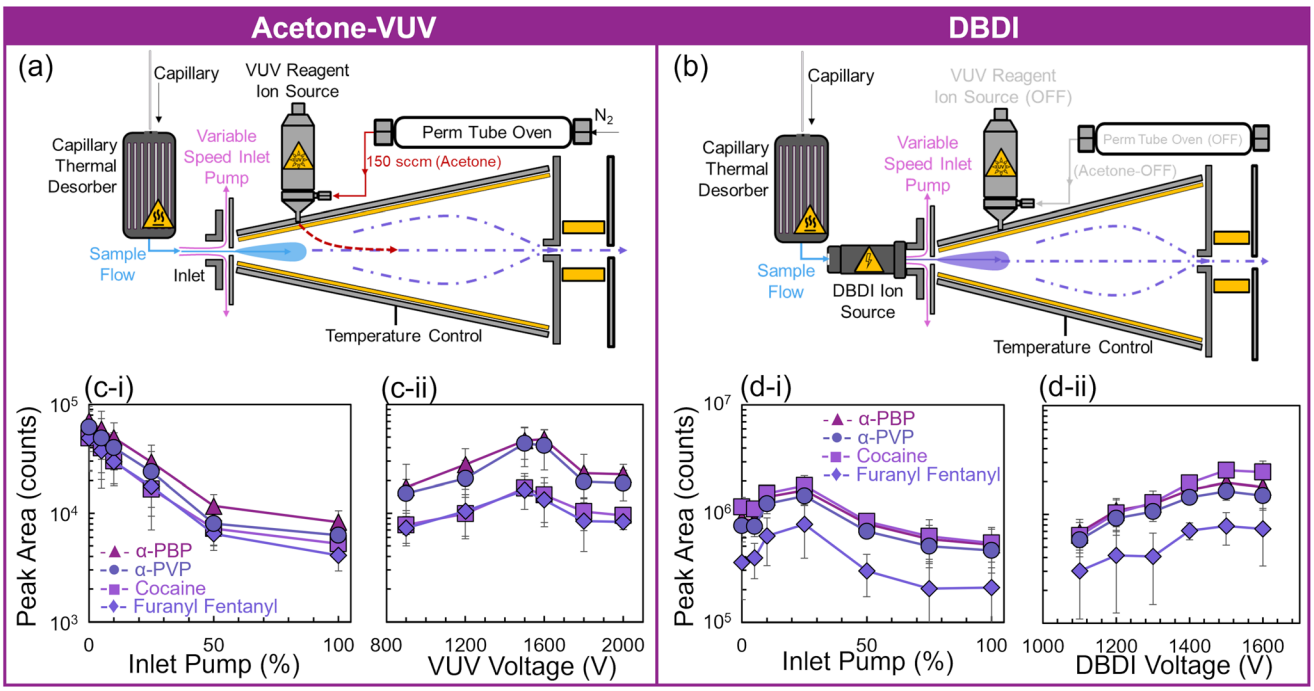

Fig. 2 Schematic representations of capillary-based thermal desorption (250 °C) coupled with (a) acetone-VUV ionization [ion-molecule reactor temp: 50 °C, perm tube flow: 150 cm^3 min^{-1}] or (b) DBDI ionization [15 kHz]. (c) and (d) Peak areas of select drugs from the 15-component mixture at 5 ng μL^{-1} (each compound) concentration as a function of (i) inlet pump flow (in percent speed [rpm] of pump) and (ii) ionization scheme (VUV or DBDI) voltage. Data points and uncertainty represented by average and standard deviation of 7–10 replicate measurements (schematics adapted from TOFWERK).[35]

through the pump, potential dilution, and in cases, elevated linear velocities reducing analyte-ion interaction time and overall ionization efficiency. However, the DBDI source configuration (Fig. 2(b)) exhibited a higher upstream aerodynamic resistance (*i.e.*, it contained a smaller inner diameter), which required additional pumping assistance for optimal signal (Fig. 2(d-i)). In the case of the in-line flow-through DBDI source, flow rates approaching 2.5 L min^{-1} extinguished the ionization plasma.[42] The MS response as a function of inlet pump flow was not strongly dependent on physicochemical properties of the individual drugs and generally exhibited similar trends across all compounds in the 15-component mixture. Therefore, we only plotted a subset of compounds for visibility. As the methods and instrumentation move into analyzing samples with background contamination or potential particulate collection or even direct wipe analysis, the inlet pump settings may require reevaluation. Though this study focused on solvent extracted wipes, direct thermal desorption of wipe-based samples (*i.e.*, no extraction) was demonstrated as a potential future avenue (Fig. S4†).[45,47]

Sample ionization. In addition to the proximity and interaction time between neutral analytes and primary ions, ionization was impacted by the ionization pathway, available ion density, and implementation of dopant(s) (Fig. S1†). Both ionization schemes were driven by an applied potential to initiate either a krypton lamp (acetone-VUV) or plasma discharge (DBDI). Fig. 2(c-ii) and (d-ii) display the MS response for select drugs as a function of these potentials. In general, the increase in potential led to increases in ion density and improved ionization. However, elevated applied potentials exhibited detrimental effects. For example, sufficiently high potentials with the DBDI plasma yielded some molecular fragmentation.[42] Similarly, in both cases, unnecessarily elevated potentials may lead to reductions in lamp or electrode lifetimes.

Ion transmission and detection. Dopant-assisted ionization played a major role for the VUV photoionization scheme,[48] as well as a smaller role for the DBDI scheme. An acetone permeation tube was employed for dopant-assisted VUV photoionization, which enabled proton transfer and adduct formation from photoionized acetone. Photoionization of the acetone dopant exhibited predominately the acetone dimer base peak (nominal *m*/*z* 117 $[(C_3H_6O)_2 + H]^+$) with smaller acetone monomer (nominal *m*/*z* 59 $[C_3H_6O + H]^+$) and acetone water cluster peaks (nominal *m*/*z* 77 $[C_3H_6O + H_2O + H]^+$), as displayed in Fig. 3(a-i). Gas phase reactions (detailed in ESI, eqn (S1)–(S5)†) with the analyte occurred in the temperature controlled and electric field-free region prior to the first quadrupole (Fig. 2(a)). This ionization scheme resulted in predominately protonated analyte molecules, enabling use of existing compound libraries (*e.g.*, the NIST DART Forensics Mass Spectral Library)[49] for identification. Increases in the flow of acetone produced modest increase in analyte signals (Fig. S5†). Any minor increase in signal must also be weighed in relation to reduced lifetime of the permeation tube. In addition, the distribution of acetone peaks was adjustable using the first quadrupole ion guide for filtering. Increasing the quadrupole RF amplitude (V_{RF}) decreased the overall intensity of the protonated acetone dimer (Fig. S6†) relative to the monomer and water adduct. However, this had minimal impact on the signal of analytes.

During DBDI-based experiments, the acetone permeation tube heater and carrier gas flow were off (Fig. 2(b)), however, acetone related ions (*e.g.*, protonated monomer, water adduct, and protonated dimer) were still observed (Fig. 3(b-i)). This was attributed to the volatility of acetone, its vapor pressure of ≈25 kPa at room temperature, and the vacuum suction from the reduced pressure in the ion-molecule reactor. To completely remove the acetone-related species from the system, the permeation tube and VUV lamp should be removed from the instrument and the lamp location capped. DBDI-generated hydronium clusters and excited gas species led to protonation of the analytes directly within the source (Fig. 2(b)), as well as charge exchange or proton transfer with downstream acetone vapor in the reaction region (detailed in ESI, eqn (S6)–(S13)†).[37,38]

The overall signal of the protonated acetone dimer base peak yielded similar intensity (*i.e.*, counts per second, cps) across ionization schemes (Fig. 3(a-i) and (b-i)). However, using the differing inlet pump settings for drug samples of each configuration (Fig. 2) resulted in a total ion count (TIC) for the DBDI source approximately 20 to 50 times higher. This was attributed to the additional ambient air drawn into the thermal desorber, ion source, and mass spectrometer. The increased pull of ambient laboratory air also provided additional water molecules for adducting with the acetone and acetonitrile extraction solvent. Fig. 3(a-ii) and (b-ii) display the spectra of blank acetonitrile samples, exhibiting an acetonitrile dimer (*m*/*z* 83 $[(C_2H_3N)_2 + H]^+$), dimer water cluster (*m*/*z* 101 $[(C_2H_3N)_2 + H_2O + H]^+$), and trimer water cluster (*m*/*z* 142 $[(C_2H_3N)_3 + H_2O + H]^+$). The DBDI source yielded elevated signal of the acetonitrile species and an increase in the water clusters. The increased sampling of laboratory air was also corroborated by the observation of elevated *m*/*z* 118 in the background spectrum (Fig. 3(b-i) and (b-ii)). This ion was previously identified as diethylethanolamine ($[C_6H_{15}NO + H]^+$), an HVAC corrosion inhibitor observed in the background of this specific laboratory of the Advanced Measurement Laboratory on the NIST Gaithersburg campus.

Both sources maintained similar analyte ionization, yielding protonated molecules of all compounds in the 15-drug mixture, with some minor solvent-based or dopant-based adduct formation. Fig. 3(a-iii) and (b-iii) display the background subtracted spectra of the 15-component mixture. Peak identifications were numbered as listed in Table 1. The chromatography-free nature of this platform prohibited the differentiation of the two sets of isomers in the mixture. In addition, slight differences in the temporal separation of species between the two ion source configurations were observed (Fig. 3(c) and (d)). For example, the acetone-VUV configuration yielded more significant overlap (in time) between the solvent peaks associated with the acetonitrile solvent and the 'early'

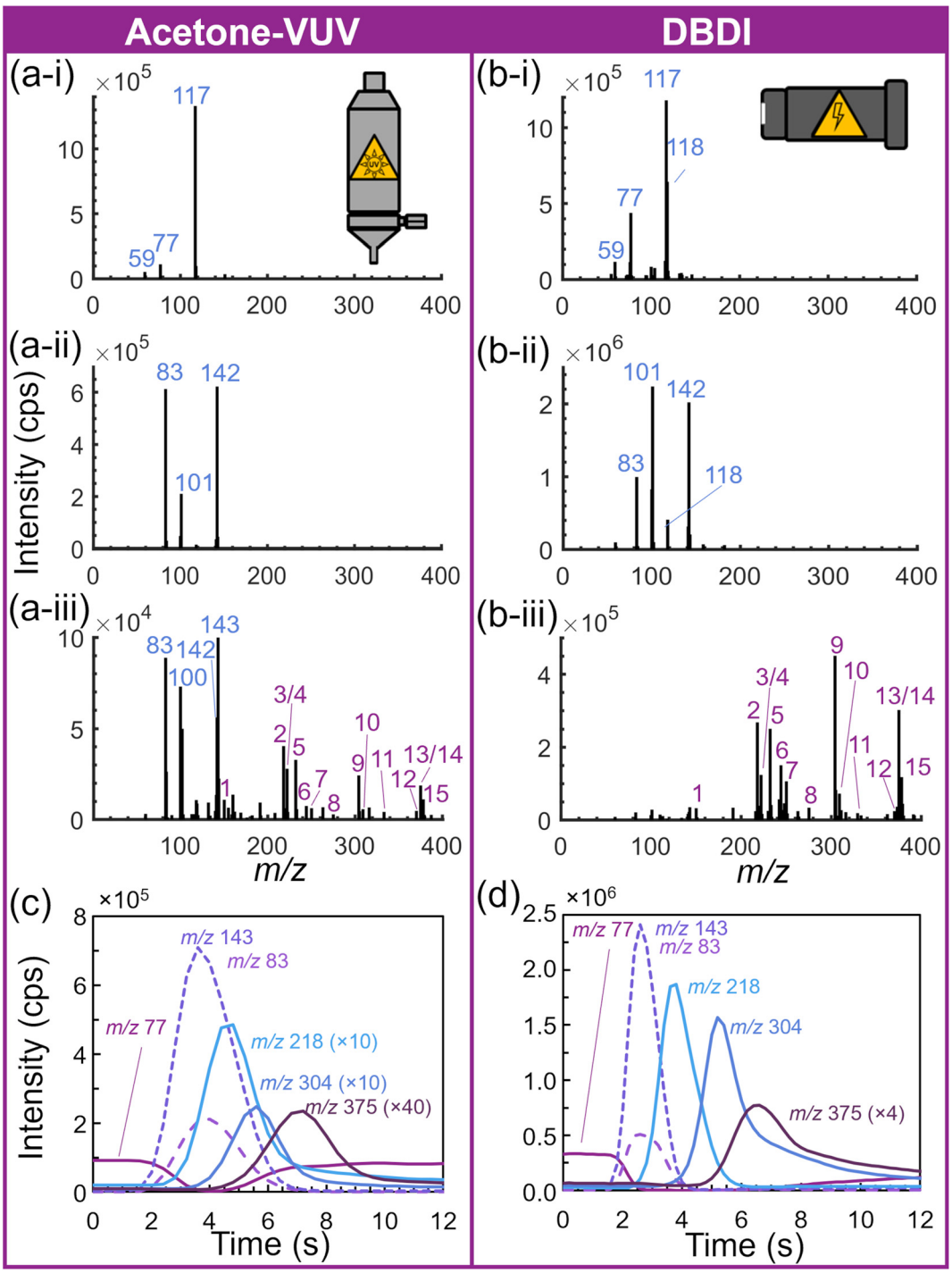

Fig. 3 Mass spectra and extracted ion chronograms for (a) acetone-assisted VUV photoionization and (b) DBDI ionization configurations. Spectra display (i) background (ii) blank acetonitrile, and (iii) 15-component drug mixture [peak numbers 1–15 identified in Table 1] ion distributions. Blank acetonitrile spectra were background subtracted and the drug mixture spectra were blank acetonitrile subtracted. Extracted ion chronograms for the acetone water cluster (*m/z* 77), acetonitrile dimer (*m/z* 83) and cluster (*m/z* 143), α-PBP (*m/z* 218), cocaine (*m/z* 304), and furanyl fentanyl (*m/z* 375) from (c) acetone-VUV and (d) DBDI.

drug mixture components (Fig. 3(c)). However, the solvent peaks were readily separable from the drug mixture when employing the DBDI configuration (Fig. 3(b-iii) and (d)). The combination of additional competitive ionization with the extraction (or dissolution) solvent (*e.g.*, acetonitrile) and indications of poorer ionization efficiency, led to lower overall signal for the drug mixtures (*i.e.*, fewer counts). The components of the drug mixture exhibited from 2× to 24× more

Table 1 MS analysis of 15-component drug mixture, including observed ions, mixture ratios, and LOD_{90} values (calculated by ASTM E2677[50]) for both acetone-assisted VUV photoionization and DBDI ionization sources

#	Compound	Theoretical $[M + H]^+$ m/z	Mixture ratio	Acetone-VUV LOD_{90} [95% upper CI] (ng μL^{-1})	DBDI LOD_{90} [95% upper CI] (ng μL^{-1})
1	Methamphetamine	150.1283	1 : 15	0.08 [0.20]	0.09 [0.26]
2	α-PBP	218.1545	1 : 15	0.10 [0.34]	0.16 [0.27]
3	Ethylone[a]	222.1130	2 : 15	0.04 [0.10]	0.07 [0.16]
4	Butylone[a]				
5	α-PVP	232.1701	1 : 15	0.07 [0.20]	0.06 [0.16]
6	PCP	244.2065	1 : 15	0.08 [0.21]	0.20 [0.36]
7	Tenocyclidine	250.1629	1 : 15	0.48 [1.15]	0.21 [0.38]
8	Nandrolone	275.2011	1 : 15	0.45 [0.76]	0.29 [0.57]
9	Cocaine	304.1549	1 : 15	0.08 [0.21]	0.23 [0.41]
10	Alprazolam	309.0907	1 : 15	0.06 [0.13]	0.07 [0.19]
11	Stanozolol	329.2593	1 : 15	0.08 [0.19][b]	0.45 [0.75]
12	Heroin	370.1654	1 : 15	0.24 [0.44]	0.80 [1.49]
13	Furanyl fentanyl [a]	375.2073	2 : 15	0.05 [0.11]	0.04 [0.08]
14	Furanyl fentanyl 3-furancarboxamide isomer[a]				
15	5-Fluoro ADB	378.2193	1 : 15	0.05 [0.11]	0.07 [0.16]

[a] Compounds are isomers and undifferentiable in current implementation. [b] Stanozolol with acetone-VUV exhibited improved sensitivity for an acetone adduct, m/z 387.3012 $[M + C_3H_7O]^+$.

counts from the DBDI source, with an overall average of approximately 10× more counts. Interestingly, with the differences in background, overall limits of detection were still similar.

Detection performance. We concluded the characterization of process parameters impacting MS detection with a cursory look at compound sensitivity. Overall analyte sensitivity may depend on a range of uncontrolled parameters, including ambient environment, background, interfering compounds, and various matrix effects. Here, we provided a quantitative estimate of drug sensitivities by employing the ASTM E2677 standard test method for determining limits of detection in explosive trace detectors on a 15-component drug mixture.[50] Peak areas of each compound were extracted and analyzed across a range of mixture concentrations ([0, 0.1, 0.5, 1, 5, 10] ng μL^{-1}). Table 1 displays the mixture concentration that yielded 90% probability of detection (*i.e.*, LOD_{90}) for each compound with both front-end configurations. It is important to note that these results represented the detection of each drug in the presence of fourteen (14) other compounds of equal concentration, and therefore were subjected to potential matrix effects, specifically competitive ionization. The presence of environmental interferents, impurities, reaction byproducts, solvents, excipients, and dilutants is likely to impact analysis of actual samples. In addition, the two sets of isomers were indistinguishable here, leading to a sensitivity measure for a slightly different 2 : 15 mixture ratio relative to the 1 : 15 ratio the remaining compounds experienced.

The drug components of the mixture generally exhibited similar sensitivities across ionization schemes, demonstrating the dominance of the mass analyzer performance in overall sensitivity. Sensitivities generally fell in the tens to hundreds of picograms per microliter. Sample withdrawal by melting point capillary dipping was estimated on the order of a single microliter, yielding overall mass sensitivities of tens to hundreds of picograms. The detection of minor components in complex mixtures is critical for the analysis of drug samples and paraphernalia residues. Most compounds (from both ionization schemes) yielded linear response curves across the concentration range ([0, 0.1, 0.5, 1, 5, 10] ng μL^{-1}) investigated for sensitivity calculations (Fig. S7 and S8†). Indications of competitive ionization – based on non-linearity in the response curve at higher concentrations – were observed for methamphetamine and the combined ethylone/butylone components with the DBDI configuration (Fig. S8†). Both signal suppression and signal enhancement matrix effects were observed from the analysis of mixtures. For example, with the DBDI configuration, methamphetamine exhibited signal suppression, while the cocaine peak areas were enhanced from analysis within the 15-component mixture (Fig. S9†). Matrix effects are a universal consideration for chromatography-free mass spectrometry and generally compound specific, based on properties such as proton affinity and ionization energy.[51,52]

Compound identification CPPs

To this point, our investigations largely considered process parameters impacting MS detection. We next focused on parameters and methods impacting compound identification. Our cause-and-effect analysis generally associated these factors with mass analysis, mass calibration, and library matching (Fig. S1† – final three branches). The high mass resolution afforded by the time-of-flight mass analyzer played a significant role in compound identification through library matching algorithms.

Mass calibration. An appropriate mass calibration was required to utilize the time-of-flight mass resolution. We investigated two mass calibration options, considering the mass accuracy of a series of drugs both as single-component analytes and part of the 15-component mixture (Table S1†). The first calibration was comprised of simply the three most abun-

dant acetone dopant peaks observed. These peaks were in all spectra and of significant intensity. These mass calibrations were completed in the post processing software (Tofware, TOFWERK AG). Mass calibration from the three acetone peaks yielded mass accuracies of $\Delta m/z$ 0.003 Da (20 ppm [measured mass/exact mass]) up to 0.025 Da (66 ppm) from single-component analytes, with peaks closer to the calibrant peaks (*e.g.*, methamphetamine: m/z 150.1283) demonstrating higher mass accuracy than those further (*e.g.*, furanyl fentanyl: m/z 375.2073) (Table S1†). The next calibration incorporated the three acetone peaks in addition to a series of eight (8) to ten (10) select peaks from a polyethylene glycol (PEG-600) solution (10 ng mL^{-1}). The PEG calibrant expanded the calibration m/z coverage (up through the range considered, m/z 400), improving overall mass accuracy. PEG calibrant spectra were collected at both the beginning and end of a specific sample run (*i.e.*, data collection file). The updated calibration yielded mass accuracies of $\Delta m/z$ −0.00018 Da (−1.2 ppm) up to 0.01 Da (26 ppm) from single-component analytes (Table S2†) with a comparable range for the mixture.

Compound identification. We then investigated preliminary compound identification with the two main platform configurations (Fig. 2(a) and (b)) of single-component analytes using library matching. Here, library matching was achieved using the NIST/NIJ DART-MS data interpretation tool (DIT version 3)[53,54] and the associated NIST DART-MS forensics database (MS Library Version: Inchworm).[49,55] The collected mass spectrum of each drug compound was saved as a text file and then loaded into the DIT in place of the low in-source collision induced dissociation (isCID) spectrum. In general, the DIT accommodates multiple spectra from multiple fragmentation levels to improve matching. This will be discussed further below. We employed search parameters that limited matching to peaks with a relative intensity above 4% and within a mass tolerance of ±0.005 Da (unless noted). Table 2 provides the results from a select series of single-component drug samples analyzed and searched with the NIST/NIJ DIT. The DIT provided several spectral match scoring metrics, including, mass differences ($\Delta m/z$), fraction of peak intensity explained (FPIE), reverse match factor (RevMF), and isotope ratio difference (IRD). Details of the various metrics can be found in the literature and within the DIT web-interface.[53,54] For simplicity, we focused on the mass difference and RevMF, which was calculated as the cosine similarity between the library spectrum vector relative to an analyte vector consisting of only those peaks within a mass tolerance window (*i.e.*, ±2× user defined mass tolerance) of the library spectrum peaks. Table 2 demonstrates all the compounds identified using the DIT. Except for furanyl fentanyl and heroin with the DBDI source configuration, all compound base peaks were measured within ±0.005 Da. Most of the compounds also exhibited reverse match factors close to the ideal value of 1 (Table 2 & examples in Fig. 4(a) and Fig. S10†). The two notable exceptions, heroin and tenocyclidine, yielded poor match factors due to the nature of their respective library spectra. The helium DART-MS library spectrum for heroin (30 V setting) exhibited a base peak for the heroin fragment at m/z 310.1443 instead of the protonated molecule, m/z 370.1654, as observed here (Fig. 4(b)). Yet, heroin remained the only match for the protonated molecule the spectrum generated here. Similarly, the tenocyclidine library spectrum exhibited a base peak for the fragment at m/z 86.0970 (Fig. S10(c)†). The utility of spectral pattern matching and high mass resolution enabled accurate compound identifications (preliminary) and differentiation of certain isobaric species – for example tenocyclidine and *N*,*N*-DMP, in separate single-component samples (Table 2 & Fig. S11†). However, both compounds were not fully resolvable in a mixture of the two (Fig. S11(d)†). As the contribution of both compounds shifted the nominal m/z 250 peak, matching this peak in the DIT was beyond the default mass tolerance. In this particular case, tenocyclidine was still matched by the fragments at m/z 86.0963 and m/z 165.0730.

Finally, a set of three samples from the NIST RaDAR program were analyzed and searched against the DIT and associated library. These samples were collected in March 2024 at various harm reduction sites and extracted upon receipt at NIST. Two of the samples (referred to as RaDAR samples #1 and #2) yielded high intensity signals and strong

Table 2 Single-component drug compounds identified by the DIT, including theoretical protonated molecule m/z, observed m/z, mass error, and reverse match factor score for acetone-assisted VUV photoionization and DBDI configurations

		Acetone-VUV			DBDI		
Compound	Theoretical $[M + H]^+$ (m/z)	Observed $[M + H]^+$	$\Delta m/z$ (Da)	Match (RevMF)	Observed $[M + H]^+$	$\Delta m/z$ (Da)	Match (RevMF)
α-PBP	218.1545	218.1518	−0.0027	0.973	218.1560	0.0015	0.973
Alprazolam	309.0907	309.0876	−0.0031	0.993	309.0884	−0.0023	0.995
Cocaine	304.1549	304.1594	0.0045	0.985	304.1501	−0.0048	0.995
Fentanyl	337.2280	337.2262	−0.0018	0.993	337.2250	−0.0030	0.992
Furanyl fentanyl	375.2073	375.2023	−0.0050	0.981	375.2008	−0.0065[a]	0.985
Heroin	370.1654	370.1610	−0.0044	0.332	370.1577	−0.0077[a]	0.325
Methamphetamine	150.1283	150.1275	−0.0008	0.930	150.1282	−0.0001	0.927
N,*N*-Dimethylpentylone	250.1443	250.1435	−0.0008	0.961	250.1422	−0.0021	0.971
Tenocyclidine	250.1629	250.1636	0.0007	0.540	250.1651	0.0022	0.442

[a] Tolerance window was opened to ±0.008 Da.

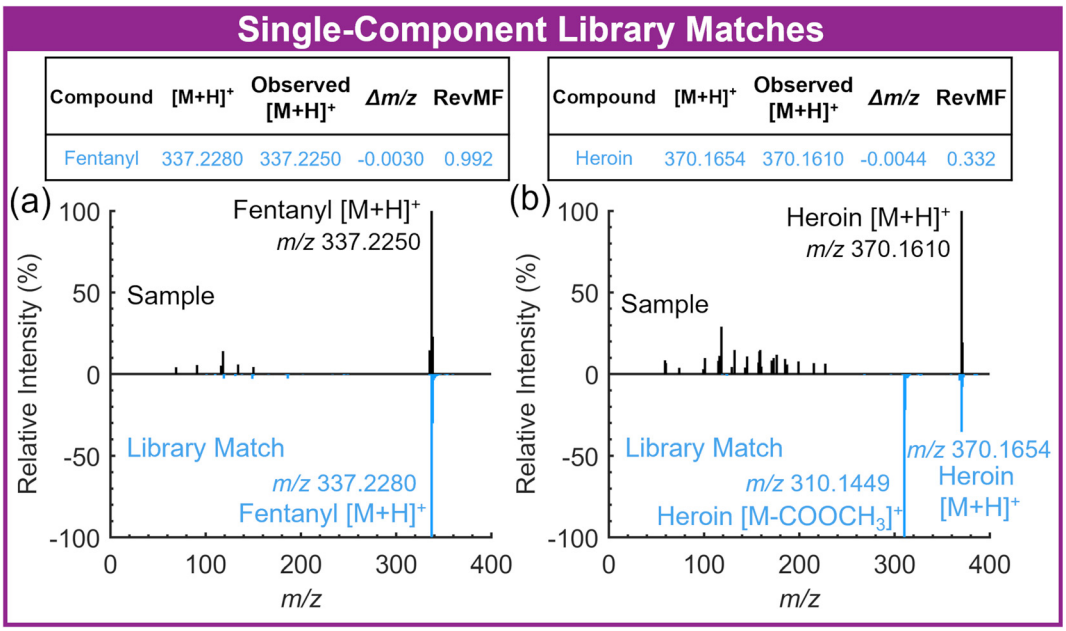

Fig. 4 Single-spectrum matching (*i.e.*, low fragmentation) of (a) fentanyl [DBDI parameters: TD: 250 °C, DBDI voltage: 1400 V, DBDI frequency: 15 kHz, inlet pump: 25%] and (b) heroin [acetone-assisted VUV photoionization parameters: ion-molecule reactor temp: 50 °C, perm tube flow: 150 cm^3 min^{-1}, VUV voltage: 1600 V, inlet pump: 5%] using the DIT with NIST DART-MS Forensics Database library. DIT search results and match factors displayed in insets.

match scores (*e.g.*, RevMF) for methamphetamine and cocaine, respectively (Fig. S12†). These findings were confirmed against previous analyses using DART-MS as outlined in the literature.[10] Fig. 5 displays the mass spectrum and identified compounds for the final RaDAR sample (#3), which exhibited several target peak matches. The mixture included fentanyl, fluorofentanyl, and the precursor 4-anilino-*N*-phenethylpiperidine (4-ANPP), all confirmed by previous analyses. The common diluent mannitol was also observed. Similar to the previous analysis, the poorer reverse match factor for mannitol (*i.e.*, 0.533) was attributed to the numerous additional fragment peaks in the mannitol library spectrum (Fig. S13†).

The high-resolution time-of-flight mass analyzer used here enabled effective compound identification, predominately targeting the protonated molecule library matching of individual spectra. As interferences increase and the analysis of mixtures becomes more complex, this may be insufficient. The DIT and NIST Forensics MS library were created for matching a series of spectra at increasing fragmentation energies – specifically for systems without tandem MS capabilities. In these cases, isCID can be applied at a target location in the differentially pumped region, increasing the frequency and energy of collisions between incoming ions and remaining gas molecules. We conducted a preliminary investigation of isCID with the present system (Fig. S14†). The quadrupole ion guide configuration allowed for increasing voltages between the skimmer after the solid rod quadrupole and the second quadrupole (Fig. S15(a)†). Ions were driven by the voltage drop in this region. Low levels of fragmentation were achieved, sufficient to completely fragment the acetone dimer (or similar dopant

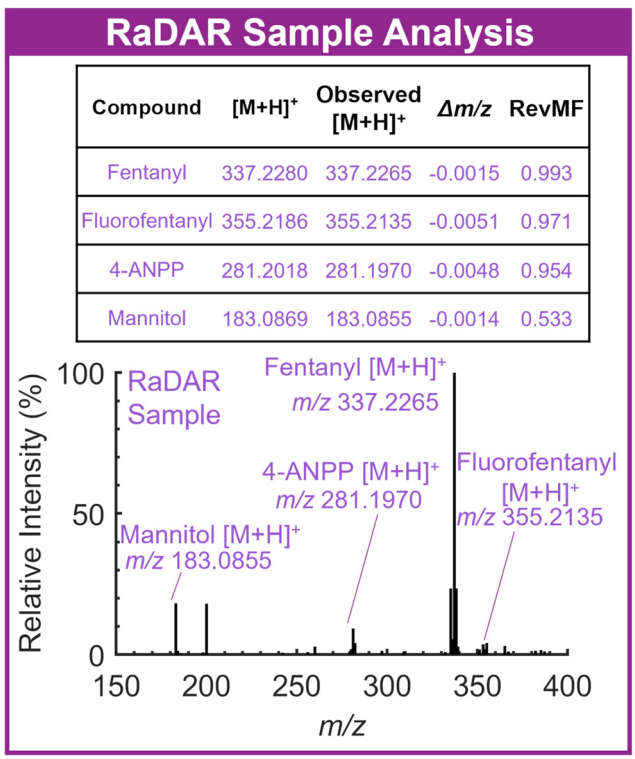

Fig. 5 Low fragmentation DBDI-MS mass spectra of RaDAR sample #3 with matched compounds labeled. Insets display search results and match scores from the DIT. Parameters: TD: 250 °C, DBDI voltage: 1400 V, DBDI frequency: 15 kHz, inlet pump: 25%.

adducts),[56] but only partially fragment larger molecules such as cocaine (Fig. S14†). This level of fragmentation was insufficient to match the corresponding spectra of the DIT. To take full advantage of the DIT and existing libraries, an alternative quadrupole configuration was considered (Fig. S15(b)†). The solid rod quadrupole 1 was replaced with a short segmented quadrupole (SSQ) allowing a DC gradient to be generated and enabling a DC-only field to be applied across the skimmer-second quadrupole isCID region. The updated quadrupole configuration enabled sufficient isCID to fragment intact drugs (*e.g.*, cocaine and fentanyl) to the extent observed in the library (Fig. S16†). Future work is aimed at optimizing the voltages necessary to match the NIST Forensics MS Library fragmentation levels more accurately.

Conclusions

In this work, we initiated development of a framework that will encompass technology characterization, advancement, and deployment pipelines, specifically targeting preliminary drug identification at the point-of-need for public health and forensic applications. Here, we focused on the analytical investigation of multiple ionization sources coupled with a rugged and transportable time-of-flight mass spectrometer. A range of parameters impacting MS detection were characterized, ultimately yielding sensitive detection (tens to hundreds of picograms) of numerous drug compounds from multicomponent mixtures (at 1 : 15 to 2 : 15 mass ratios). Mass calibration and library matching avenues were also examined, demonstrating compatibility with existing forensics-focused libraries (*i.e.*, NIST DART-MS forensics database) and search algorithms (*i.e.*, NIST/NIJ DART-MS data interpretation tool). The foundation presented here seeks to help build a framework to lower implementation barriers for new technologies and support community adoption.

Ongoing work is expanding the transportable TOF avenue into alternative ambient ionization sources such as DART and ASAP (atmospheric solids analysis probe). This initial work was focused on sources not requiring helium and operational without the need for an external rough pump (though modest signal improvement could be achieved with additional flow). However, DART configurations employing nitrogen gas (instead of helium) or using pulsed helium gas have been introduced. The need (or not) for additional gas tanks must be considered in mobile and fieldable applications. In addition, potential atmospheric conditions (*e.g.* temperature, humidity, wind currents) must be accounted for in sample introduction of ambient ion sources (*e.g.*, DART). Ongoing development of a mobile laboratory related to this work will include a temperature-controlled work environment for sample analysis on-site. Investigation of alternative mass analyzers (*e.g.*, single quadrupole and triple quadrupole) and fieldable analytical techniques (*e.g.*, Fourier transform infrared spectroscopy and novel absorption spectroscopy instruments) is also underway for applicability to point-of-need drug analysis. Future work might also consider a thermal desorption ramp as a possible means of temporally differentiating isobars. In parallel with fit-for-purpose analytical investigations, rigorous workflow validation, implementation, and documentation are in progress for deployment within a mobile laboratory setting.

Associated content

Data availability

Raw data files, derived data files, extracted peak areas, and mass spectra are available on the NIST Public Data Repository: **https://doi.org/10.18434/mds2-3591**.

Conflicts of interest

The authors declare no competing financial interests.

Acknowledgements

AK was employed by TOFWERK, the manufacturer of the Vocus S mass spectrometer used here, during the completion of this study. Official contribution of the National Institute of Standards and Technology; not subject to copyright in the United States.

References

1 E. Sisco, *Drug Detection, Analysis, and Monitoring Workshop Report*, Special Publication (NIST SP), National Institute of Standards and Technology, Gaithersburg, MD, 2024.
2 B. W. Kammrath, P. E. Leary and J. A. Reffner, Forensic Applications of Portable Spectrometers, in *Portable Spectroscopy and Spectrometry*, 2021, pp. 125–147.
3 T. P. Forbes and R. Burks, Field-Deployable Devices, in *Encyclopedia of Forensic Sciences, Third Edition*, ed. M. M. Houck, Elsevier, 3rd edn, 2023, pp. 413–423.
4 M. Philp and S. Fu, A review of chemical 'spot' tests: A presumptive illicit drug identification technique, *Drug Test. Anal.*, 2018, **10**, 95–108.
5 E. Sisco, D. F. Nestadt, M. B. Bloom, K. E. Schneider, R. A. Elkasabany, S. Rouhani and S. G. Sherman, Understanding sensitivity and cross-reactivity of xylazine lateral flow immunoassay test strips for drug checking applications, *Drug Test. Anal.*, 2024, **16**, 942–947.
6 G. Musile, Y. Agard, L. Wang, E. F. De Palo, B. McCord and F. Tagliaro, Paper-based microfluidic devices: On-site tools for crime scene investigation, *TrAC, Trends Anal. Chem.*, 2021, **143**, 116406.
7 M. Hargreaves, Handheld Raman, SERS, and SORS, in *Portable Spectroscopy and Spectrometry*, 2021, pp. 347–376.
8 E. Sisco, A. Burns, E. Schneider, C. R. Miller IV and L. Bobka, Comparing two seized drug workflows for the

analysis of synthetic cannabinoids, cathinones, and opioids, *J. Forensic Sci.*, 2022, **67**, 471–482.
9 S. E. Rodriguez-Cruz, Evaluating the sensitivity, stability, and cross-reactivity of commercial fentanyl immunoassay test strips, *J. Forensic Sci.*, 2023, **68**, 1555–1569.
10 M. G. Appley, E. L. Robinson, A. Thomson, E. Russell and E. Sisco, An analytical platform for near real-time drug landscape monitoring using paraphernalia residues, *Forensic Chem.*, 2023, **34**, 100489.
11 S. A. Borden, A. Saatchi, G. W. Vandergrift, J. Palaty, M. Lysyshyn and C. G. Gill, A new quantitative drug checking technology for harm reduction: Pilot study in Vancouver, Canada using paper spray mass spectrometry, *Drug Alcohol Rev.*, 2022, **41**, 410–418.
12 H. West, J. Fitzgerald, K. Hopkins, E. Li, N. Clark, S. Tzanetis, S. L. Greene and G. E. Reid, Early Warning System for Illicit Drug Use at Large Public Events: Trace Residue Analysis of Discarded Drug Packaging Samples, *J. Am. Soc. Mass Spectrom.*, 2021, **32**, 2604–2614.
13 D. T. Snyder, C. J. Pulliam, Z. Ouyang and R. G. Cooks, Miniature and Fieldable Mass Spectrometers: Recent Advances, *Anal. Chem.*, 2016, **88**, 2–29.
14 H. M. Brown, T. J. McDaniel, P. W. Fedick and C. C. Mulligan, The current role of mass spectrometry in forensics and future prospects, *Anal. Met.*, 2020, **12**, 3974–3997.
15 K. Evans-Nguyen, A. R. Stelmack, P. C. Clowser, J. M. Holtz and C. C. Mulligan, Fieldable Mass Spectrometry for Forensic Science, Homeland Security, and Defense Applications, *Mass Spectrom. Rev.*, 2021, **40**, 628–646.
16 K. H. Blakeman and S. E. Miller, Development of High-Pressure Mass Spectrometry for Handheld and Benchtop Analyzers, in *Portable Spectroscopy and Spectrometry*, 2021, pp. 391–413.
17 C. J. Brais, J. O. Ibañez, A. J. Schwartz and S. J. Ray, Recent Advances in Instrumental Approaches to Time-of-Flight Mass Spectrometry, *Mass Spectrom. Rev.*, 2021, **40**, 647–669.
18 T. I. Yacovitch, B. M. Lerner, M. R. Canagaratna, C. Daube, R. M. Healy, J. M. Wang, E. C. Fortner, F. Majluf, M. S. Claflin, J. R. Roscioli, E. M. Lunny and S. C. Herndon, Mobile Laboratory Investigations of Industrial Point Source Emissions during the MOOSE Field Campaign, *Atmosphere*, 2023, **14**, 1632.
19 M. E. Monge, G. A. Harris, P. Dwivedi and F. M. Fernandez, Mass Spectrometry: Recent Advances in Direct Open Air Surface Sampling/Ionization, *Chem. Rev.*, 2013, **113**, 2269–2308.
20 S. Rankin-Turner, P. Sears and L. M. Heaney, Applications of ambient ionization mass spectrometry in 2022: An annual review, *Anal. Sci. Adv.*, 2023, **4**, 133–153.
21 C. L. Feider, A. Krieger, R. J. DeHoog and L. S. Eberlin, Ambient Ionization Mass Spectrometry: Recent Developments and Applications, *Anal. Chem.*, 2019, **91**, 4266–4290.
22 Z. E. Lawton, A. Traub, W. L. Fatigante, J. Mancias, A. E. O'Leary, S. E. Hall, J. R. Wieland, H. Oberacher, M. C. Gizzi and C. C. Mulligan, Analytical Validation of a Portable Mass Spectrometer Featuring Interchangeable, Ambient Ionization Sources for High Throughput Forensic Evidence Screening, *J. Am. Soc. Mass Spectrom.*, 2017, **28**, 1048–1059.
23 S. Mathias, M. Amerio-Cox, T. Jackson, D. Douce, A. Sage, P. Luke, R. Sleeman, C. Crean and P. Sears, Selectivity of Explosives Analysis with Ambient Ionization Single Quadrupole Mass Spectrometry: Implications for Trace Detection, *J. Am. Soc. Mass Spectrom.*, 2024, **35**, 50–61.
24 S. Mathias, M. Amerio-Cox, T. Jackson, D. Douce, B. McCullough, A. Sage, P. Luke, C. Crean and P. Sears, Performance Comparison of Ambient Ionization Techniques Using a Single Quadrupole Mass Spectrometer for the Analysis of Amino Acids, Drugs, and Explosives, *J. Am. Soc. Mass Spectrom.*, 2024, **35**, 2480–2489.
25 E. Sisco and T. P. Forbes, Forensic applications of DART-MS: A review of recent literature, *Forensic Chem.*, 2021, **22**, 100294.
26 M. d. M. Boronat Ena, D. A. Cowan and V. Abbate, Ambient ionization mass spectrometry applied to new psychoactive substance analysis, *Mass Spectrom. Rev.*, 2023, **42**, 3–34.
27 T. P. Forbes and E. Sisco, Recent advances in ambient mass spectrometry of trace explosives, *Analyst*, 2018, **143**, 1948–1969.
28 H.R.1734 - TRANQ Research Act of 2023, Public Law 118-23, (12/19/2023), 118th Congress, U.S. Government Publishing Office, **https://www.congress.gov/bill/118th-congress/house-bill/1734/text**.
29 Biden-Harris Administration Designates Fentanyl Combined with Xylazine as an Emerging Threat to the United States. Office of National Drug Control Policy, U.S. White House Press Release, 2023. **https://www.whitehouse.gov/ondcp/briefing-room/2023/04/12/biden-harris-administration-designates-fentanyl-combined-with-xylazine-as-an-emerging-threat-to-the-united-states/**(accessed 2024, Sept. 4).
30 E. Russell, E. Sisco, A. Thomson, J. Lopes, M. Rybak, M. Burnett, D. Heilman, M. G. Appley and R. M. Gladden, Rapid Analysis of Drugs: A Pilot Surveillance System To Detect Changes in the Illicit Drug Supply To Guide Timely Harm Reduction Responses—Eight Syringe Services Programs, Maryland, November 2021–August 2022, *Morb. Mortal. Wkly. Rep.*, 2023, **72**, 458–462.
31 Rapid Drug Analysis and Research (RaDAR): Providing Near Real-Time Insight into the Illicit Drug Landscape. National Institute of Standards and Technology, **https://www.nist.gov/programs-projects/rapid-drug-analysis-and-research-radar-providing-near-real-time-insight-illicit** (accessed 2025, March 11).
32 G. I. Gkatzelis, M. M. Coggon, B. C. McDonald, J. Peischl, J. B. Gilman, K. C. Aikin, M. A. Robinson, F. Canonaco, A. S. H. Prevot, M. Trainer and C. Warneke, Observations Confirm that Volatile Chemical Products Are a Major Source of Petrochemical Emissions in U.S. Cities, *Environ. Sci. Technol.*, 2021, **55**, 4332–4343.
33 D. Fillion, S. Perrier, M. Riva, C. George, F. Domine and R.-M. Couture, Emission of Volatile Organic Compounds to the Atmosphere from Photochemistry in Thermokarst

Ponds in Subarctic Canada, *ACS Earth Space Chem.*, 2024, **8**, 563–574.
34 M. M. Nudnova, L. Zhu and R. Zenobi, Active capillary plasma source for ambient mass spectrometry, *Rapid Commun. Mass Spectrom.*, 2012, **26**, 1447–1452.
35 M. Riva, V. Pospisilova, C. Frege, S. Perrier, P. Bansal, S. Jorga, P. Sturm, J. Thornton, U. Rohner and F. Lopez-Hilfiker, Evaluation of a reduced pressure chemical ion reactor utilizing adduct ionization for the detection of gaseous organic and inorganic species, *Atmos. Meas. Tech.*, 2024, **17**, 5887–5901.
36 L. Gyr, F. D. Klute, J. Franzke and R. Zenobi, Characterization of a Nitrogen-Based Dielectric Barrier Discharge Ionization Source for Mass Spectrometry Reveals Factors Important for Soft Ionization, *Anal. Chem.*, 2019, **91**, 6865–6871.
37 M. Weber, J.-C. Wolf and C. Haisch, Effect of Dopants and Gas-Phase Composition on Ionization Behavior and Efficiency in Dielectric Barrier Discharge Ionization, *J. Am. Soc. Mass Spectrom.*, 2023, **34**, 538–549.
38 J.-C. Wolf, L. Gyr, M. F. Mirabelli, M. Schaer, P. Siegenthaler and R. Zenobi, A Radical-Mediated Pathway for the Formation of [M + H]+ in Dielectric Barrier Discharge Ionization, *J. Am. Soc. Mass Spectrom.*, 2016, **27**, 1468–1475.
39 J. L. Staymates, M. E. Staymates and J. Lawrence, The effect of reusing wipes for particle collection, *Int. J. Ion Mobil. Spectrom.*, 2015, **19**, 41–49.
40 J. R. Verkouteren, J. L. Coleman, R. A. Fletcher, W. J. Smith, G. A. Klouda and G. Gillen, A method to determine collection efficiency of particles by swipe sampling, *Meas. Sci. Technol.*, 2008, **19**, 115101.
41 D. Fisher, R. Zach, Y. Matana, P. Elia, S. Shustack, Y. Sharon and Y. Zeiri, Bomb swab: Can trace explosive particle sampling and detection be improved?, *Talanta*, 2017, **174**, 92–99.
42 T. P. Forbes, E. L. Robinson, E. Sisco and A. Koss, In-Line Thermal Desorption and Dielectric Barrier Discharge Ionization for Rapid Mass Spectrometry Detection of Explosives, *Anal. Chem.*, 2024, **96**, 13352–13357.
43 E. Sisco and T. P. Forbes, Rapid detection of sugar alcohol precursors and corresponding nitrate ester explosives using direct analysis in real time mass spectrometry, *Analyst*, 2015, **140**, 2785–2796.
44 E. Sisco and T. P. Forbes, Direct analysis in real time mass spectrometry of potential by-products from homemade nitrate ester explosive synthesis, *Talanta*, 2016, **150**, 177–183.
45 E. Sisco, M. E. Staymates and T. P. Forbes, Optimization of confined direct analysis in real time mass spectrometry (DART-MS), *Analyst*, 2020, **145**, 2743–2750.
46 T. P. Forbes and S. T. Krauss, Confined DART-MS for Rapid Chemical Analysis of Electronic Cigarette Aerosols and Spiked Drugs, *J. Am. Soc. Mass Spectrom.*, 2021, **32**, 2274–2280.
47 E. Sisco, T. P. Forbes, M. E. Staymates and G. Gillen, Rapid analysis of trace drugs and metabolites using a thermal desorption DART-MS configuration, *Anal. Methods*, 2016, **8**, 6494–6499.
48 S. Wang, W. Wang, H. Li, Y. Xing, K. Hou and H. Li, Rapid On-Site Detection of Illegal Drugs in Complex Matrix by Thermal Desorption Acetone-Assisted Photoionization Miniature Ion Trap Mass Spectrometer, *Anal. Chem.*, 2019, **91**, 3845–3851.
49 E. Sisco and A. S. Moorthy, *NIST DART-MS Forensics Database (is-CID)*, National Institute of Standards and Technology, 2020, DOI: **10.18434/mds2-2313**.
50 ASTM E2677 Limit of Detection Web Portal, 2014. **https://www-s.nist.gov/loda/**, (accessed 20162016).
51 E. H. Denis, J. L. Bade, R. S. Renslow, K. A. Morrison, M. K. Nims, N. Govind and R. G. Ewing, Proton Affinity Values of Fentanyl and Fentanyl Analogues Pertinent to Ambient Ionization and Detection, *J. Am. Soc. Mass Spectrom.*, 2022, **33**, 482–490.
52 J. T. Shelley and G. M. Hieftje, Ionization matrix effects in plasma-based ambient mass spectrometry sources, *J. Anal. At. Spectrom.*, 2010, **25**, 345–350.
53 A. S. Moorthy, S. S. Tennyson and E. Sisco, Updates to the Inverted Library Search Algorithm for Mixture Analysis, *J. Am. Soc. Mass Spectrom.*, 2022, **33**, 1260–1266.
54 E. Sisco, A. S. Moorthy, S. S. Tennyson and R. Corzo, *NIST/NIJ DART-MS Data Interpretation Tool*, National Institute of Standards and Technology, 2021, DOI: **10.18434/mds2-2448**.
55 A. N. Couch, J. Sharp and J. T. Davidson, Assessing the effectiveness of the NIST DART-MS Forensics Database and Data Interpretation Tool for designer drug screening with alternative instrumentation, *Int. J. Mass Spectrom.*, 2023, **483**, 116964.
56 F. D. Lopez-Hilfiker, S. Iyer, C. Mohr, B. H. Lee, E. L. D'Ambro, T. Kurtén and J. A. Thornton, Constraining the sensitivity of iodide adduct chemical ionization mass spectrometry to multifunctional organic molecules using the collision limit and thermodynamic stability of iodide ion adducts, *Atmos. Meas. Tech.*, 2016, **9**, 1505–1512.